Journal of Sound and Vibration (2003) **259**(5), 1131–1146
doi:10.1006/jsvi.2002.5119, available online at http://www.idealibrary.com on IDEAL®

VIBRATION-BASED DAMAGE IDENTIFICATION USING RECONSTRUCTED FRFS IN COMPOSITE STRUCTURES

H.-Y. Kim

Agency for Defense Development (ADD), Propulsion System Department, Technical Research Center, P.O. Box 35, *Yousung, Tajeon City* 305-600, *Republic of Korea.*
E-mail: *hyukim@postech.ac.kr*

(*Received* 11 *September* 2001, *and in final form* 16 *April* 2002)

This work aims to establish a vibration-based damage identification method for fiber-reinforced laminated composites and their sandwich construction. This new on-line structural damage identification technique uses the structural dynamic system reconstruction method exploiting the frequency response functions (FRFs) of a damaged structure. To verify the effectiveness of this damage identification method, the frequency responses obtained by vibration testing of fatigue-damaged laminated composites and honeycomb sandwich beams with debonding are examined according to the extent of the damage via the fatigue-damage load cycle for laminated composites, and via the debonding extent for honeycomb sandwich beams. The changes of the peaks and valley of the FRFs according to the debonding extent and the fatigue load cycles are examined, and the area changes in the FRFs are also discussed as the damage index. The residual FRFs or the difference between intact and damaged FRFs are newly defined for application of the on-line damage identification method. Finally, the delamination extent for the sandwich beams and the fatigue damage level for the laminated composites can be easily identified in terms of the changes in natural frequencies and damping ratios of the reconstructed FRFs for these damaged composite structures.

1. INTRODUCTION

The most common damage identification methods used today are visual inspection and localized experimental methods, such as acoustic or ultrasonic methods, which require that the location of the damage be known *a priori* and be readily accessible. The need for quantitative global damage detection methods applicable to complex structures has led to methods that examine changes in the vibration characteristics of the structures. Research in this field has been spurred by several factors: catastrophic failures resulting in loss of life, such as in-flight failure of aircraft structural components; the economics of repairing aging infrastructures; advances in digital signature analysis techniques such as modal testing and system identification methods. In vibration-based damage identification, the changes in the modal parameters of beams, plates, and even rather complicated truss and bridge structures, can be exploited using the finite element model of these structures for diverse structural damages.

Many researchers have investigated the global damage identification methods, mostly based on changes on the vibrational characteristics, from various aspects: frequency changes in terms of forward problems [1–3], and of inverse problems [4–6]; mode shape displacement or curvature/strain changes [7–9]. Changes on flexibility or stiffness matrix are also used for the damage identification: flexibility changes [10]; stiffness error matrix

0022-460X/02/$35.00

method [11]; changes in measured stiffness matrix [12]. Some researchers implement the iterative optimization methods to efficiently identify the damages in structures: structural model parameter updating [13]; optimal matrix method [14–16]; sensitivity-based update method [17–19]; eigenstructure assignment method [20, 21].

Model-based damage identification techniques are generally used to monitor changes in structural dynamic characteristics or changes in the dynamical response of structures. Combined with modal analysis, these techniques provide global as well as local damage information. The reference model for an undamaged structure is built using finite element analysis (FEA). However, FEA-based damage identification methods have many limitations. Some can detect only pre-specified forms of damage in their diagnostic schemes. FEA-based methods usually compare the undamaged structural parameters with the damage information, but the reference structural model is not consistent because of aging and variation in the operational environment. FEA-based methods also often fail to detect small defects in global structures [22]. Moreover, a large number of sensors or measurement points are needed to locate damage accurately on a large structure. FEA-based damage identification methods are therefore liable to be inaccurate and expensive: In most of the previous works, the finite element model has been adopted for the damaged structures so that FEA-based damage identification is limited in its application to in-service structures. Also, as more and more structures are made from composite material, there are a lot of research works in the area of identification of mechanical properties of composite structures based on vibration rather than FEA [23–26].

On-line damage identification is increasingly popular because of more stringent requirements in the integrity and safety assessment of structures. The idea is to identify damage as soon as it is initiated, to monitor continuously the health of the structure without affecting its operation, and if possible to rectify the damage. Research works on on-line vibration-based monitoring and diagnostics of a structure are recently focused: optimization [27] and modal norms [28] of frequency response functions (FRFs) of the damaged structures. Natke and Cempel [29] used the symptoms as sensitive quantities of a defect/fault/damage in the operational systems undergoing aging, wear, etc. They introduced and manipulated the observation matrix for the evaluation of symptoms in the context of the state-space formulation.

There is hardly any research paper available in the open literature dealing with the damage identification based on the state-space system reconstruction of the measured FRFs in the modal co-ordinate. This paper provides a new vibration-based damage identification method using the reconstructed subspace system model, which is obtained from differences in the frequency responses of healthy and damaged structures. To develop an on-line damage identification method, the structural dynamic system reconstruction methods which accurately provide modal parameter estimates are employed to obtain the modal parameters of the damaged structures. In application, the frequency responses are used of fatigue-damaged composite laminate beams and of debonded honeycomb sandwich beams. The extent of the damage in these composite structures can be identified from the natural frequencies and damping ratios of the reconstructed dynamic system; these are also compared with a damage indicator, namely the normalized area change of the measured FRF curves.

2. EXPERIMENTS

Fiber-reinforced composite laminates and their sandwich beams were fabricated to demonstrate the effectiveness of the vibration-based damage identification method. These composite beams were then tested as specified below.

2.1. MATERIAL AND SPECIMEN

For the vibration testing on the fatigue damaged beams, resin-containing carbon-fiber/epoxy prepreg having the physical properties shown in Table 1 was used to produce composite plates with a lay-up $[90_2/0_2]_s$. The curing cycle was 1·5 h at 130°C, with a warming-up cycle of 0·5 h at 80°C.

The test specimens were cut to dimensions 20 mm × 300 mm × 1 mm from the laminate plates by a diamond cutter, following the ASTM D-3039/D-3470 standards. To avoid stress concentration in the gripping area, glass-fiber/epoxy tab material was bonded by adhesive to each end of the specimen.

To study the effect of face-layer debonding on the vibrational characteristics of honeycomb sandwich beams, sandwich beams with skin laminates of carbon-fiber/epoxy composite were fabricated using an autoclave and vacuum bag cure. The skin laminate was pre-cured and subsequently bonded to core. Each layer of adhesive has a thickness of 0·005 in and a density of 1153 kg/m^3. To produce good quality sandwich beams reliably, cure cycle was adopted as follows: 1 h from the ambient temperature to 125°C, 1·5 h at 125°C, and 1 h from 125°C to the ambient temperature. The honeycomb sandwich beams are made of Nomex aramid honeycomb core supplied by Hexcel Composites. The honeycomb core has a nominal cell size of 3 mm and a core thickness of 19 mm. Mechanical properties of the honeycomb core are listed in Table 2. The properties of the face layers are the same as that of the fatigue-damaged beams.

The face-skin laminate panels of thickness 1 mm with a lay-up $[0_2/90_2]_s$ for the honeycomb sandwich construction are cut into beams using a diamond wheel cutter. A width b of 45 mm was chosen to be greater than twice the sandwich height and three times the cell size as recommended by the ASTM standards [30]. The honeycomb core was cut with the ribbon direction in the longitudinal direction along the beam axis. Debonded sandwich beams were made by inserting teflon films of various sizes between the face layer and the honeycomb core.

2.2. EXPERIMENTAL PROCEDURE

A fatigue testing was performed first, to investigate the reduction in stiffness of composite laminates due to the extensional fatigue loading. Vibration testing was performed to obtain the natural frequencies of the cantilever-beam-type laminates that had been subjected to the fatigue loading. Figure 1 shows the fatigue and vibration testings. Before fatigue testing, tensile strength test was carried out in an Shimadzu UTM

TABLE 1

Properties of carbon/epoxy prepreg (USN125 Type A)

Properties	Value
Young's modulus in fiber direction (E_1)	$120{\cdot}3 \times 10^9$ Pa
Young's modulus in transverse direction (E_2)	$7{\cdot}63 \times 10^9$ Pa
Shear modulus (G_{12})	$3{\cdot}36 \times 10^9$ Pa
The Poisson ratio (μ_{12})	0·32
Volume density (ρ)	1510 kg/m^3
Tensile strength in fiber direction (X_T)	$2{\cdot}2 \times 10^9$ Pa
Compressive strength in fiber direction (X_C)	$1{\cdot}4 \times 10^9$ Pa
Tensile strength in traverse direction (Y_T)	$2{\cdot}1 \times 10^6$ Pa
Compressive strength in traverse direction (Y_C)	$1{\cdot}3 \times 10^9$ Pa
Ply shear strength in fiber direction (S)	$0{\cdot}226 \times 10^9$ Pa

TABLE 2

Properties of honeycomb core (Hexel aramid)

Properties	Type A Type B
Density (kg/m^3)	96·1 80·1
Shear strength in longitudinal direction (F_x)	$2{\cdot}28 \times 10^6$ Pa $1{\cdot}90 \times 10^6$ Pa
Shear modulus in longitudinal direction (G_x)	$89{\cdot}6 \times 10^6$ Pa $70{\cdot}3 \times 10^6$ Pa
Shear strength in width direction (F_y)	$1{\cdot}38 \times 10^6$ Pa $1{\cdot}21 \times 10^6$ Pa
Shear modulus in width direction (G_y)	$44{\cdot}8 \times 10^6$ Pa $37{\cdot}2 \times 10^6$ Pa

machine with a 20 kN load cell. The experiments were performed in displacement-control mode at a stroke rate of 2 mm/min, and the longitudinal displacements were measured by the Autograph. The average extensional modulus and ultimate strength of three specimens are measured as 61·49 GPa and 845·65 MPa respectively. Fatigue tests were then performed by the Servopulser in load-control mode. The cyclic loading profile applied in fatigue tests was a pure sinusoidal wave of 3 Hz having three different maximum loading levels, 50, 60 and 70% of tensile strength. A minimum loading of 5% ultimate strength was applied to prevent possible compression loading. For each loading level, all specimens were categorized according to specified cycles, and every three specimens were subjected to fatigue loading for these cycles.

Vibration testing was performed using an HP-3566A FFT spectrum analyzer with a data-acquisition personal computer. The vibration tests shown in Figure 2 were conducted using the sandwich cantilever beam specimens damaged by debonding. A Dytran-5800SL instrumented impulse hammer was used to hit the cantilever beam laminate sample. The impact took place at the end of the cantilever beam to reduce the excitation of higher vibrational modes. A Kaman-KD2300 proximity sensor was located at the end of the laminate beam to measure the displacement. The force and displacement signals were processed by a digital Fourier transform algorithm in the analyzer to convert the discrete time signals into frequency-domain data. The FRFs were displayed, as voltage ratios between the displacement response and force excitation in the frequency domain, on a computer monitor. Each distinct vibration test was performed 10 times to provide an averaged frequency response function. Natural frequencies were observed from the plot of the FRF by eye, using a pointing cursor to pick the resonance points. For the fatigue damage analysis of the laminated beams, the frequencies of three specimens having the same fatigue damage cycles were averaged to reduce frequency error due to variation in the specimen dimension and properties.

3. FRF RECONSTRUCTION OF DAMAGED STRUCTURES

The structural dynamic system reconstruction is based on the subspace identification for the use of vibration spectral estimates, which can provide the reconstructed transfer functions in terms of the modal parameter for the transfer function poles and zeros. This section outlines the structural dynamic system reconstruction method, detailed in reference [31]. The system matrix estimates are derived using the observability matrix and the input

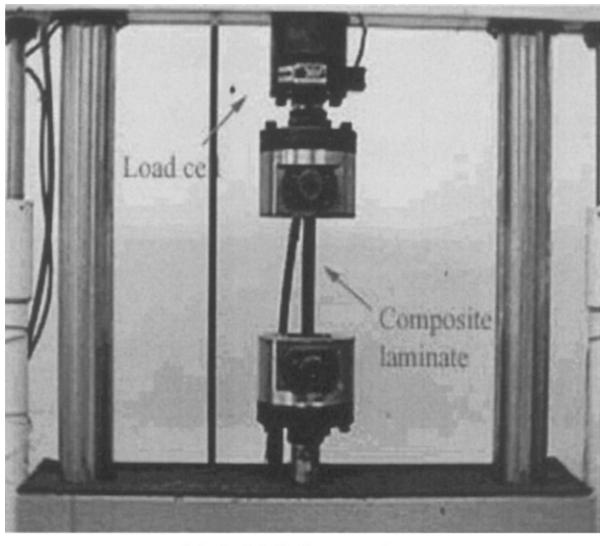

(a) Axial-fatigue testing

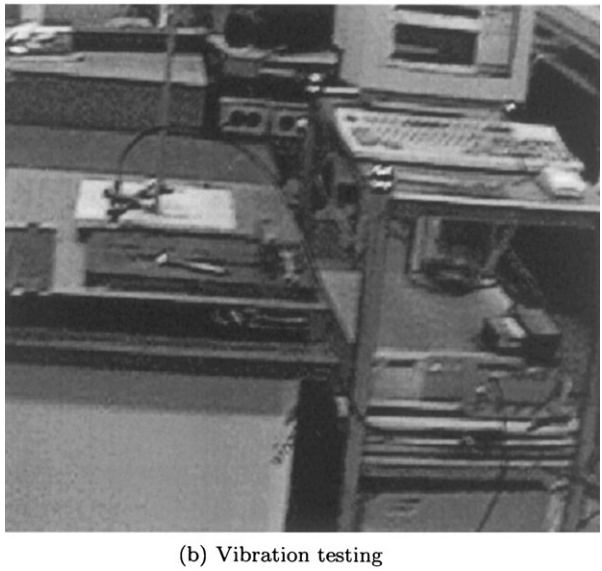

(b) Vibration testing

Figure 1. Photographs of experimental set-ups for the axial-fatigue and vibration test.

participation matrix is estimated from the system matrix parameterization for the frequency-domain input–output relationships.

The spectrum estimates from the noisy input and output data are given by the smoothed periodograms comprising the frequency contents of the signal over a finite time interval [32]. To analyze the smoothed periodograms, define the residual spectrum estimate $\mathscr{S}_q$ and the frequency shift matrix I_q to obtain the observability range space, defined by the linear vector subspace ranged by the system observability matrix $\mathscr{O}_q$:

$$\mathscr{S}_q \triangleq \mathscr{S}_{yy} - \mathscr{S}_{yu}\mathscr{S}_{uu}^{\dagger}\mathscr{S}_{yu}^{\mathrm{H}}, \tag{1}$$

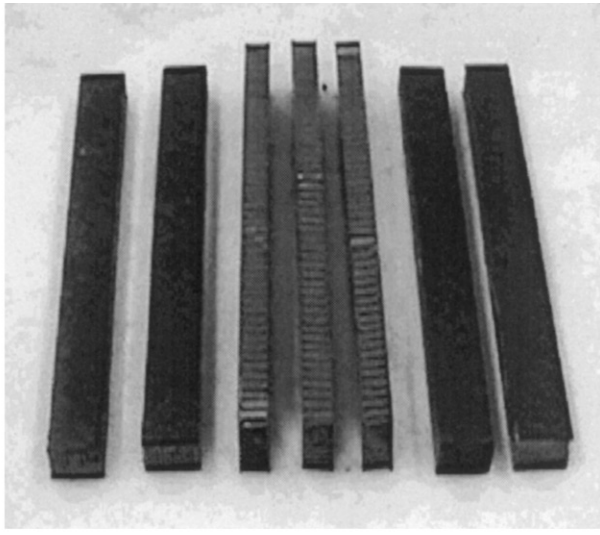

(a) Honeycomb sandwich beam specimens

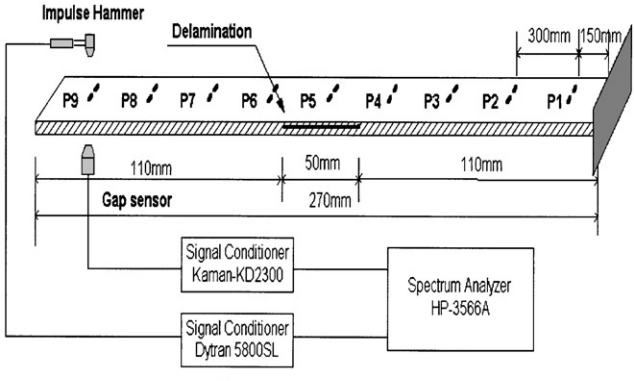

(b) Experimental configuration

Figure 2. Photograph of honeycomb sandwich beams and configuration of experimental set-up for vibration testing.

where

$$\{\mathscr{S}_{yy}, \mathscr{S}_{uu}, \mathscr{S}_{yu}\} = \sum_{z=1}^{M} I_q(z) \otimes \{S_{yy}^M(z), S_{uu}^M(z), S_{yu}^M(z)\} \tag{2}$$

and

$$I_q(z) \triangleq \begin{bmatrix} 1 & e^{-j2\pi z/M} & \cdots & e^{-j2\pi(q-1)z/M} \\ e^{j2\pi z/M} & 1 & \cdots & e^{j2\pi(q-2)z/M} \\ \vdots & \vdots & \vdots & \vdots \\ e^{j2\pi(q-1)z/M} & \cdots & \cdots & 1 \end{bmatrix}. \tag{3}$$

Here, the superscript † denotes the Moore–Penrose inverse and $\otimes$ denotes the Kronecker product of the matrices.

When the system is minimal and the observability matrix $\mathcal{O}_q$ is non-singular, it is well known that the estimate of the system matrix A can be obtained from the observability matrix and its submatrices [33]: $A = \mathcal{O}_{q-1}^{\dagger}\bar{\mathcal{O}}_{q-1}$, where

$$\mathcal{O}_{q-1} = \begin{bmatrix} C \\ CA \\ \vdots \\ CA^{q-2} \end{bmatrix}, \qquad \bar{\mathcal{O}}_{q-1} = \begin{bmatrix} CA \\ CA^2 \\ \vdots \\ CA^{q-1} \end{bmatrix}. \tag{4}$$

With the singular-value decomposition (SVD) of the residual spectral estimate, the basis vectors of the range space of $\mathcal{O}_q$ can be computed as follows:

$$\Re[\mathcal{S}_q] = [U \quad U_{n_x}] \begin{bmatrix} \Sigma & \mathbf{0} \\ \mathbf{0} & \Sigma_n \end{bmatrix} \begin{Bmatrix} U \\ U_{n_x} \end{Bmatrix}, \tag{5}$$

where $[U \;\; U_{n_x}] \in \mathscr{R}^{qn_y \times qn_y}$ is the unitary matrix, and $\mathrm{diag}[\Sigma \;\; \Sigma_n] = \mathrm{diag}[\ldots, \sigma_{n_x+i}, \ldots] \in \mathscr{R}^{qn_y \times qn_y}$ is the diagonal matrix of singular values σ_{n_x+i}, $i = 1, \ldots, qn_y - n_x$.

The integer n_x is the number of orders about a specified singular-value threshold $\bar{\sigma}$ such that

$$\sigma_i > \bar{\sigma}, \quad i = 1, \ldots, n_x \text{ and } \sigma_{n_x+i} < \bar{\sigma}, \quad i = 1, \ldots, qn_y - n_x. \tag{6}$$

The basis vector matrix of the observability range space can be estimated as $U \in \mathscr{R}^{qn_y \times n_x}$. By combining the truncated unitary matrix U in equation (5) with the observability matrix $\mathcal{O}_q$, we obtain the estimates of $\hat{A}$ and $\hat{C}$ of the subspace system identification model:

$$\hat{A} = U_{q-1}^{\dagger}\bar{U}_{q-1}, \quad \hat{C} = U_1. \tag{7}$$

From the identified system matrix $\hat{A}$ and the output matrix $\hat{C}$ in equation (7), the matrices $\hat{B}$ and $\hat{D}$ can be simply parameterized in the least-squares sense using the spectrum estimates as follows. Consider the transfer function relation between the auto-spectrum estimate S_{uu} and the output cross-spectrum estimate S_{yu}:

$$\hat{B}, \hat{D} = \arg\min_{\hat{B},\hat{D}} \left\| S_{yu}(z) - [\hat{C}(\mathrm{e}^{-\mathrm{j}2\pi z/M} I_{n_x} - \hat{A})^{-1}, I_{n_u}] \begin{bmatrix} \hat{B} \\ \hat{D} \end{bmatrix} S_{uu}(z) \right\|_F^2. \tag{8}$$

Define

$$Q(z) \triangleq [\hat{C}(\mathrm{e}^{-\mathrm{j}2\pi z/M} I_{n_x} - \hat{A})^{-1}, I_{n_u}]. \tag{9}$$

By applying Kronecker product relations, we can obtain the estimates for the matrices $\hat{B}$ and $\hat{D}$ [31]:

$$[\hat{B}, \hat{D}]^{\mathrm{T}} = \sum_{z=1}^{M} \Re([Q^{\mathrm{H}}Q]^{\dagger} Q^{\mathrm{H}} S_{yu} S_{uu}^{\mathrm{H}} [S_{uu}^{\mathrm{H}} S_{uu}]^{\dagger}), \tag{10}$$

where

$$Q(z) \triangleq [\hat{C}(\mathrm{e}^{-\mathrm{j}2\pi z/M} I_{n_x} - \hat{A})^{-1}, I_{n_u}]. \tag{11}$$

For modal analysis and damage detection in vibrating structural systems, it is often necessary to develop canonical structural dynamic models from the state-space system in terms of eigenmode parameters such as natural frequencies, damping ratios and mode shapes. First, a similarity transformation $\mathbf{x}(k) = \Psi\mathbf{z}(k)$ can be applied to the estimated

state-space system matrices to give the eigenvalue system equation

$$\mathbf{z}(k+1) = \Lambda \mathbf{z}(k) + F\mathbf{u}(k), \qquad \mathbf{y}(k) = E\mathbf{z}(k) \tag{12}$$

with

$$\Lambda = \frac{\ln(\Psi^{-1} A \Psi)}{\triangle t} = \mathrm{diag}\{\sigma_i \pm \mathrm{j}\omega_i\}, \qquad \Psi^{-1} B = \lfloor \ldots | \Re(F_i) \pm \Im(F_i)] \ldots]^{\mathrm{T}},$$
$$C\Psi = \lfloor \ldots [\Re(E_i) \pm \Im(E_i)] \ldots \rfloor, \quad i = 1, \ldots, n.$$

The similarity transformation, called the common basis-normalized structural identification method $\mathbf{z}_i = T_i \mathbf{x}_i$ ($T_i = T_i^{(2)} T_i^{(1)}$) [34], can be applied to equation (12) to obtain the mode-co-ordinate reconstructed transfer function:

$$T_i^{(1)} = \frac{c_i}{2\mathrm{j}\omega} \begin{bmatrix} -\sigma_i + \mathrm{j}\omega_i & 1 \\ \sigma_i + \mathrm{j}\omega_i & -1 \end{bmatrix}, \qquad T_i^{(2)} = \begin{bmatrix} -\sigma_i - r_i\omega_i & 1 \\ -\sigma_i^2 - \omega_i^2 & \sigma_i - r_i\omega_i \end{bmatrix}, \tag{13}$$

where $r_i = \Im F_i / \Re F_i$ and c_i is a mass normalization parameter in F_i and E_i. We have

$$\hat{A}_i = \begin{bmatrix} 0 & 1 \\ -(\omega_i^2 + \sigma_i^2) & -2\sigma_i \end{bmatrix}, \qquad [0, \hat{B}_i^{(1)}]^{\mathrm{T}} = \frac{1}{c_i} \begin{bmatrix} 0 \\ 2\Re F_i \end{bmatrix}, \tag{14}$$

$$[\hat{C}_i^{(1)}, \hat{C}_i^{(2)}] = c_i[(r_i\sigma_i - \omega_i)\Im E_i - (\sigma_i + r_i\omega_i)\Re E_i, \ \Re E_i - r_i \Im E_i]. \tag{15}$$

The reconstructed FRF for the input vector $\mathbf{u}$ and displacement output vector $\mathbf{y}$ can be represented as

$$G(\omega) = \sum_{i=1}^{n} \hat{C}_i (\omega I - \hat{A}_i)^{-1} \hat{B}_i = \sum_{i=1}^{n} \frac{2(\Re F_i)(\Re E_i) - (\Im F_i)(\Im E_i)}{\omega I - \hat{A}_i}. \tag{16}$$

The natural frequencies and damping ratios of dynamic systems can be found from the complex conjugate pairs of eigenvalues of the identification system matrix $\hat{A}_i$:

$$\sigma_i \pm \mathrm{j}\omega_i = -\zeta_i \omega_{ni} \pm \mathrm{j}\omega_{ni}\sqrt{1 - \zeta_i^2}, \tag{17}$$

or directly from the discrete eigenvalues λ_i, and $\bar{\lambda}_i$ of the estimated system matrix $\hat{A}$:

$$\sigma_i = \frac{1}{2 \triangle t} \ln(\lambda_i \bar{\lambda}_i), \qquad \omega_i = \frac{1}{\triangle t} \arctan\left[\frac{\Im \lambda_i}{\Re \lambda_i}\right]. \tag{18}$$

Moreover, the corresponding mode shapes, found from the numerators of the mode-co-ordinated reconstructed transfer function, can be obtained by applying simultaneous impulses at the position of displacement output sensors.

4. FRFS OF DAMAGED COMPOSITE STRUCTURES

FRF-based damage identification involves only the measurements from a small number of sensors located on the structure, and does not require a complex structural model. Damage is detected using vibration measurements, and identified by comparing signals in higher frequency ranges before and after damage. In on-line damage identification, the measured response functions of the operational structures have to take into account the changes of physical parameters in the structures due to damage. Global changes in stiffness and delamination in composite structures affect the FRFs in easily predictable ways, so that the natural frequencies and damping ratios of

damaged structures can readily be adopted for debonding or delamination in the structures.

The structural dynamic transfer function for a damaged structure, based on the FRF, is given as

$$G_{ij}(f) = \frac{\Psi_{ij}(f)}{\Psi_{ii}(f)} = \frac{\mathbf{h}_i^* \mathbf{h}_j}{\mathbf{h}_i^* \mathbf{h}_i}, \tag{19}$$

where $\mathbf{h}$ are the row entries of the FRF matrix for the applied excitation, and Ψ_{ij} is the cross-power spectrum. (No summation over i is implied in $\mathbf{h}_i^* \mathbf{h}_i$.) The input loads have the same relative force levels and occur at the same locations on the structure for each test. The transfer function is the ratio of the response of the cross-spectral density between input i and sensor j to the input auto-spectral density at point i. This is a non-dimensional complex quantity that specifies how vibration is transmitted between points i and j on the structure as a function of frequency. The FRFs do not depend on whether the receptance, mobility or inertance spectral densities are measured. FRF-based damage identification is accurate because the relative vibration response across small sections of the structure is characterized. The difference between FRFs is a continuous function with many peaks and valleys, and when damage occurs these peaks and valleys shift relative to each other. The sensitivity of changes in the FRF to mild damage generally increases as the actuator and sensors move closer to the damage, and as the frequency of the excitation is increased.

The area under the FRF curve can be interpreted as the possible meaning of the potential energy density of the structures under the assumption of unit inertial energy density. When the mass of the structure is unchanged by the damage, the change of stiffness can be determined from changes of the FRF-curve area. Thus, a normalized damage index matrix can be defined as

$$D = \frac{\int_{f_1}^{f_2} ||G_{ij}^d|| \, \mathrm{d}f}{\int_{f_1}^{f_2} ||G_{ij}^h|| \, \mathrm{d}f} - 1, \tag{20}$$

where the integrated is taken element by element, and the superscripts on G_{ij}^d indicate damaged (d) or healthy (h); and f denotes frequency. This damage indicator therefore lose the information on the peaks and valleys of FRF data.

In the damage-indicator equation (20), the normalized area difference of the FRF curves suggests an alternative FRF of damaged structures for damage identification. This is called the residual FRF matrix $R(\omega)$, and is defined by

$$R(\omega) \doteq G^d(\omega) - G^h(\omega). \tag{21}$$

Figure 3 presents the frequency responses and the residual FRFs of debonded honeycomb sandwich beams for the variety of debonding extent and type. The peaks of both the measured responses and their residual FRFs shift to lower frequency as the debonding extent increases in the sandwich beams. Figure 4 also shows the measured responses and residual FRFs of axial-fatigue-damaged laminated beams as a function of the number of fatigue loading cycles.

5. DAMAGE IDENTIFICATION USING RECONSTRUCTED RESIDUAL FRFS

The structural dynamic system expressed in terms of modal-parameter co-ordinates can be then obtained from the residual FRFs by using the structural dynamic system

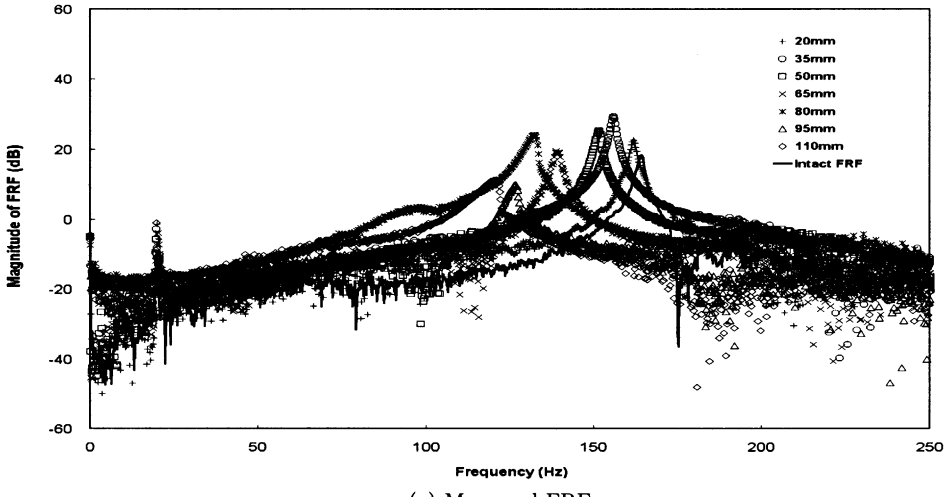

(a) Measured FRF

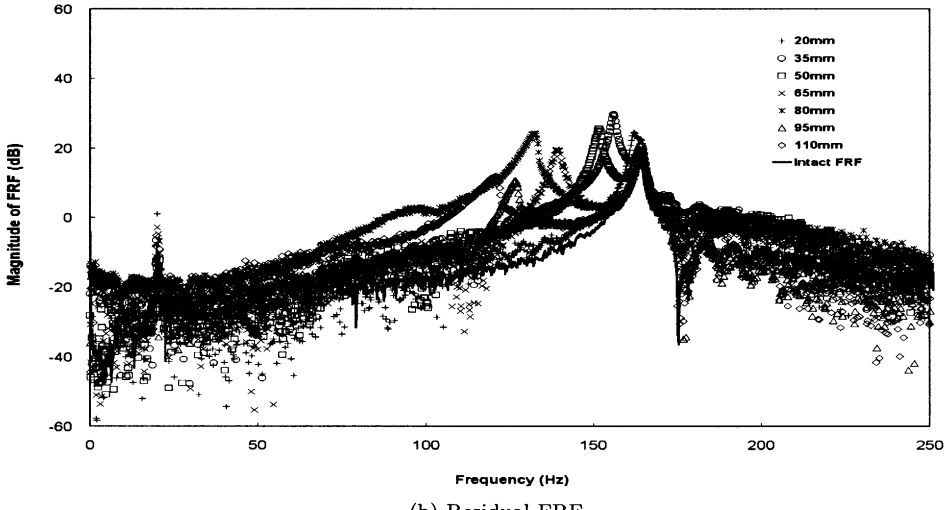

(b) Residual FRF

Figure 3. Frequency responses for the debonded honeycomb sandwich beam.

reconstruction method in section 3, as follows:

$$R(\omega) = \sum_{i=1}^{n} \frac{V_i^{res}}{\omega I - A_i^{res}}, \tag{22}$$

$$A_i^{res} = \begin{bmatrix} 0 & 1 \\ -(\omega_i^2 + \sigma_i^2) & -2\sigma_i \end{bmatrix}, \qquad V_i^{res} = 2(\Re F_i \Re E_i - \Im F_i \Im E_i),$$

where A_i^{res} and V_i^{res} are the ith-mode eigenvalue matrix and the ith-mode residue of the reconstructed dynamic system respectively. Damage can therefore be identified from changes in the eigenvalues and residues of the reconstructed structural dynamic system using equation (22).

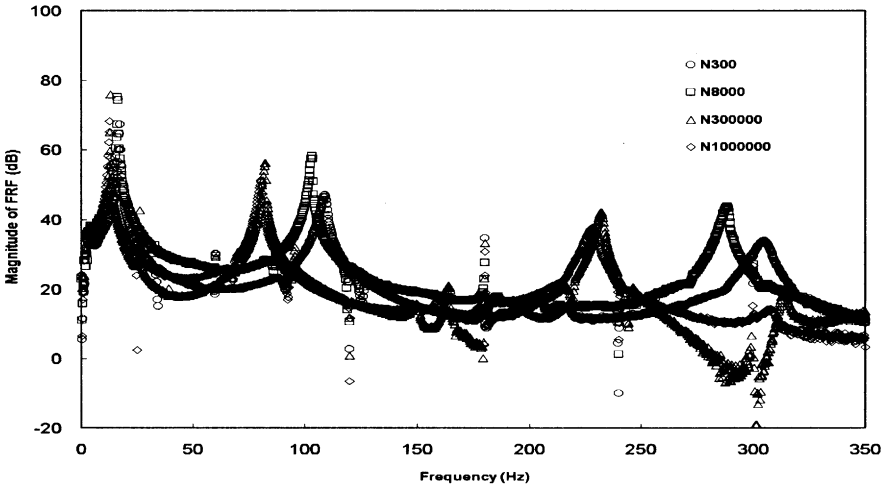

(a) Measured FRF

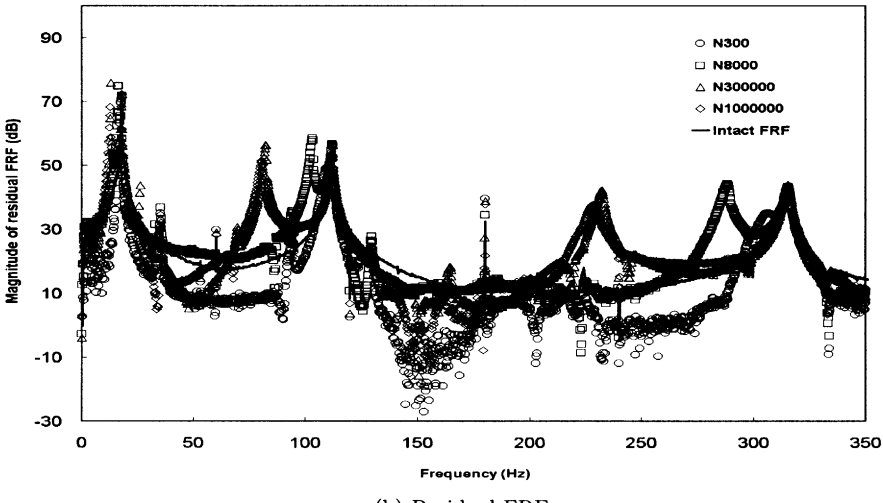

(b) Residual FRF

Figure 4. Frequency responses for the axial-fatigue-damaged laminated beams.

Figure 5 presents frequency response curves reconstructed from residual FRFs for debonded honeycomb sandwich beams with delamination lengths 50 and 110 mm. Figure 6 shows response curves of the reconstructed dynamic system for composite laminated beams damaged by extensional fatigue loads and fatigue cycle numbers 300 and 1×10^6. These figures show that the reconstructed response functions accurately capture the residual frequency responses of the damaged structures.

In Tables 3 and 4, the natural frequencies and damping ratios of the reconstructed dynamic systems for the debonded sandwich beams and the fatigue-loaded laminate beams are set out based on the dynamic system reconstruction method. A group of natural frequencies can be recognized that represent the dynamical characteristics of the intact beam; that the natural frequencies in this group decrease proportionately until a critical

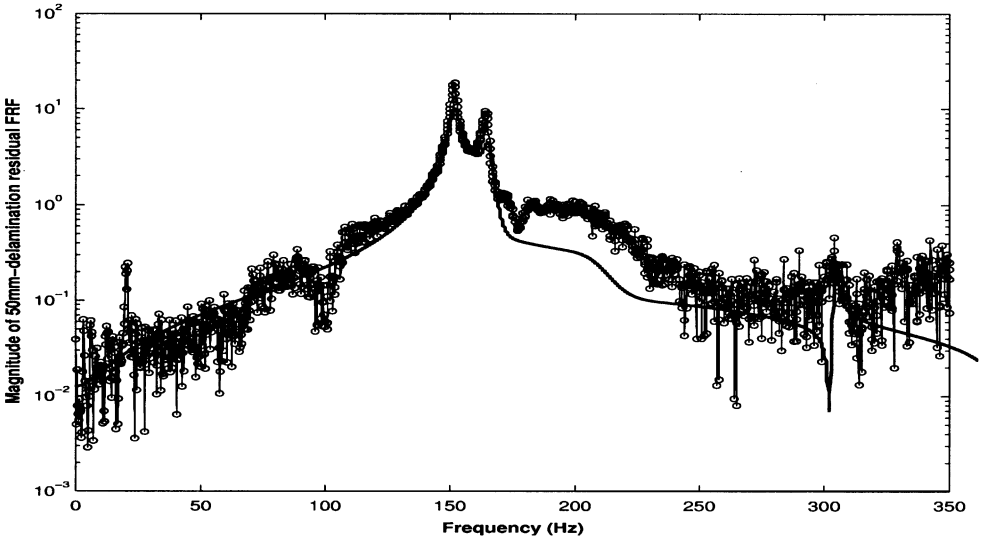

(a) FRF for 50mm delamination length

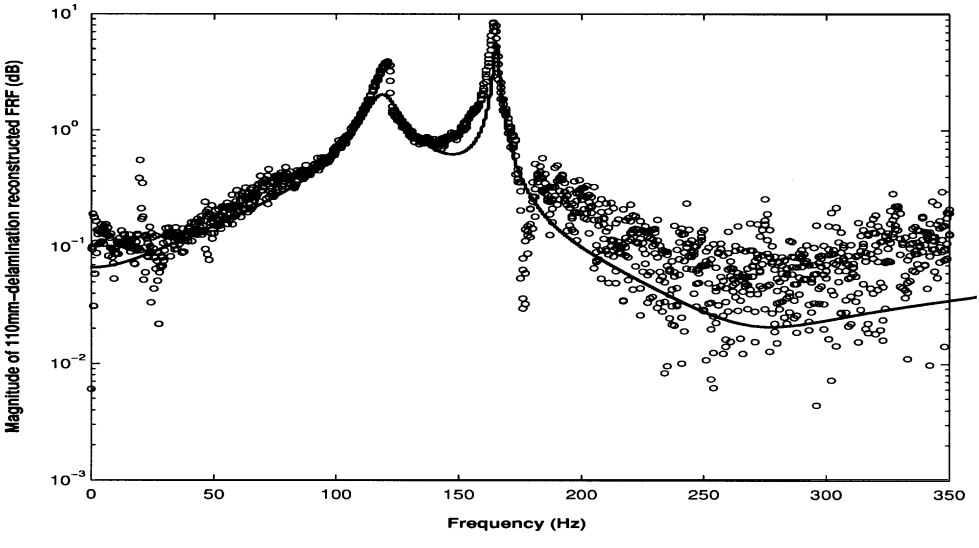

(b) FRF for 110mm delamination length

Figure 5. Reconstructed residual FRFs for the debonded honeycomb sandwich beam (measured=circles, reconstructed=solid lines).

debonding extent (marked by dagger in the tables) is reached. The damping ratios in this group show a small increase, while the natural frequency decreases. Beyond this critical debonding extent, another group of natural frequencies arise which represents the dynamical characteristics of the damaged sandwich beam, while the natural frequencies of the intact beam become invariant. The damping ratios in this group increase noticeably beyond the critical debonding extent. These damping ratios for the case of fatigue-loaded beams do not increase beyond the critical debonding extent.

The indicator D in equation (20) does not increase monotonically with the damage so that the use of this damage indicator could lead to incorrect damage information for the

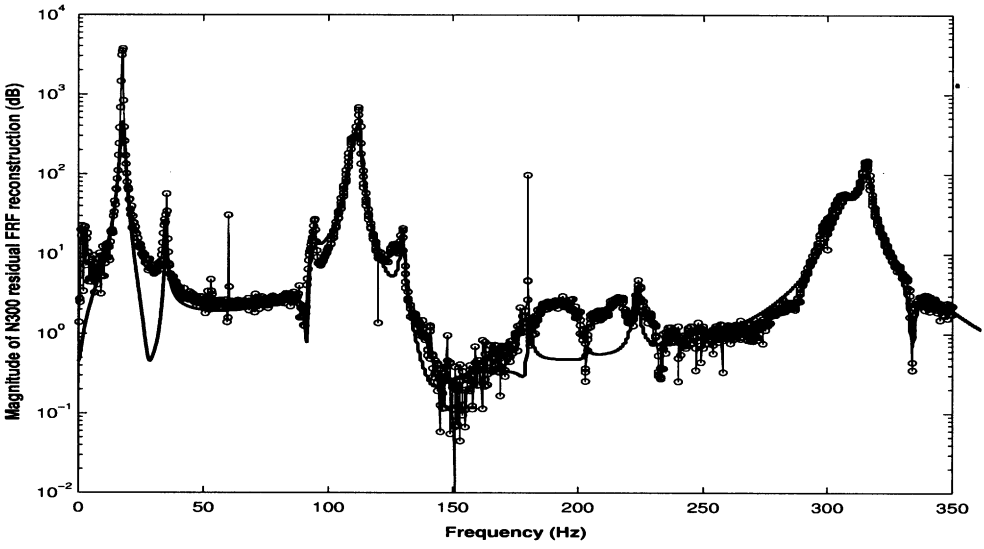

(a) FRF for 300-cycle axial fatigue

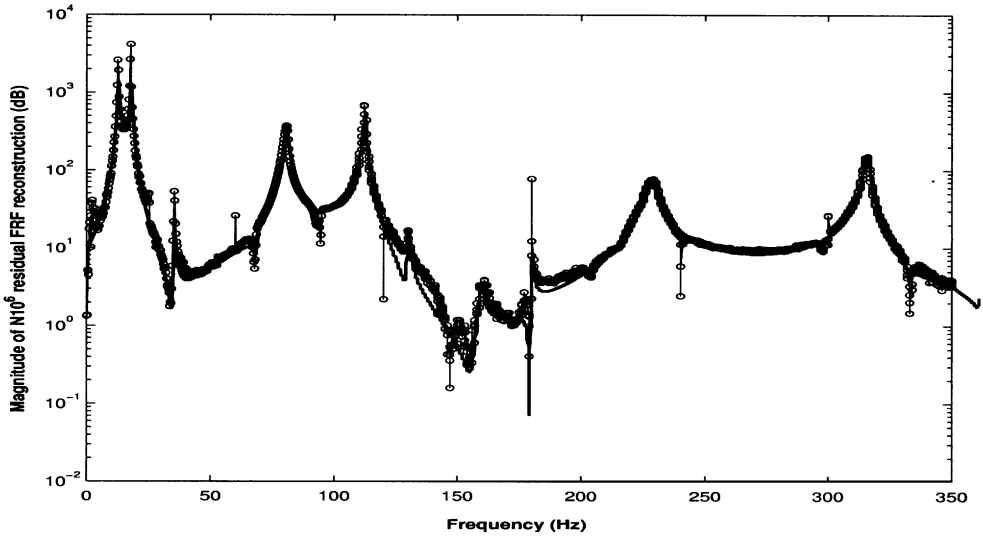

(b) FRF for 1000000-cycle axial fatigue

Figure 6. Reconstructed residual FRFs for the axial-fatigue-damaged laminated beams (measured=circles, reconstructed=solid lines).

sandwich beams. However, damage identification based on the reconstructed residual FRFs, where the differences in the natural frequencies and damping ratios of each groups are compared in order to determine the damage levels, provides reliable information on the damage extent in the sandwich beams.

In conclusion, we summarize the findings on the residual FRFs and the natural frequencies and damping ratios of the structural dynamic system reconstruction. The frequency responses and the residual FRF of the debonded honeycomb sandwich beams, and of the axial-fatigue-damaged laminated beams, show that the peaks of all response

TABLE 3

Natural frequencies and damping ratios of residual FRFs for the debonded honeycomb sandwich beams ($n_x = 30,\ q = 300$)

Debonding length	Natural frequency (Hz)	Damping ratios (%)	Normalized area deviation of FRFs
Intact	164·7	0·05	0·00
20 mm	162·6	0·05	2·11
35 mm	156·8	0·07	3·12
50 mm	151·6 (165·2)	0·12 (0·10)	2·85
65 mm	138·8 (165·0)	0·15 (0·06)	2·20
80 mm	130·9 (165·0)	0·18 (0·07)	5·32
95 mm	125·0 (165·0)	0·37 (0·06)	2·01
110 mm	118·7 (165·0)	0·54 (0·05)	2·55

TABLE 4

Natural frequencies and damping ratios of residual FRFs for fatigue-loaded composite laminates with the 70% tensile strength ($n_x = 30,\ q = 300$)

Fatigue cycle	Natural frequency (Hz)	Damping ratios (%)	Normalized area deviation of FRFs
10	17·9, 112·2, 315·5	0·18, 0·04, 0·04	0·00
300[†]	17·4, 109·4, 307·1	0·59, 0·18, 0·18	0·51
	(17·9, 112·1, 315·8)	(0·39, 0·07, 0·07)	
3×10^3	17·4, 108·0, 301·2	1·33, 0·12, 0·14	0·73
	(17·8, 112·3, 316·6)	(0·24, 0·07, 0·06)	
8×10^3	16·6, 103·1, 287·7	0·29, 0·06, 0·05	1·86
	(17·9, 112·1, 315·7)	(0·26, 0·04, 0·03)	
3×10^5	13·1, 95·0, 231·7	0·28, 0·07, 0·15	3·44
	(17·9, 112·2, 315·4)	(0·19, 0·04, 0·04)	
1×10^6	12·7, 80·5, 227·1	0·27, 0·09, 0·10	0·51
	(17·9, 112·3, 315·7)	(0·19, 0·05, 0·04)	

functions shift to lower frequency as the damage increases. Two groups of natural frequencies, representing the dynamic characteristics of the damaged and intact beams, arise before and after the damage in the structure reaches some critical level. The natural frequencies in these composite structures decrease as the debonding extent and the fatigue-load cycle increase. The change in the damping ratios with increasing damage depends on the type of damage: delamination or fatigue loaded.

6. CONCLUSION

Vibration-based damage identification has recently come to the fore due to increasing interest in the capability to monitor a structure and detect global damage at the earliest stage. For this purpose, the reconstructed residual FRF-based damage identification method has been set out. In this method, the measured FRFs depend on the physical quantities such as the reduction in stiffness due to the fatigue loading or delamination; these changes imply detectable changes in the modal, dynamical system properties.

A new damage identification method is also developed using the structural dynamic system reconstruction algorithm, based on the residual FRFs of the vibrational structures. For application of the damage identification, frequency responses for the damaged composite structures are measured to give the residual FRFs of the composites. From the FRF measurements, the effects of the damage are studied on the peaks and valley of the FRFs. Damage identification based on reconstructed residual FRFs can accurately determine the extent of the damage from the natural frequency and the damping ratios.

The damage identification methods developed here using the reconstructed residual FRFs of the damaged structures provide accurate and direct information on the damage in structures even though the damage indicator D based on the FRF-curve area is inconsistent.

REFERENCES

1. M. M. F. Yuen 1985 *Journal of Sound and Vibration* **103**, 301–310. A numerical study of the eigenparameters of a damaged cantilever.
2. H. Sato 1983 *Journal of Sound and Vibration* **89**, 59–64. Free vibration of beams with abrupt changes of cross section.
3. J. E. T. Penny, M. I. Friswell and D. A. L. Wilson 1994 *Modal Analysis: International Journal of Analytical and Experimental Modal Analysis* **9**, 239–254. Using vibration data and statistical measures to locate damage in structures.
4. S. Hassitos and G. D. Jeong 1993 *Composite Structures* **49**, 679–691. Assessment of structural damage from natural frequency measurements.
5. L. M. See, C. G. Koh and T. Balendra 1995 *Journal of Structural Engineering* **121**, 1155–1160. Damage detection of building: numerical and experimental studies.
6. A. Morassi and N. Rovere 1997 *Journal of Engineering Mechanics* **123**, 422–432. Localizing a notch in a steel frame from frequency measurements.
7. K. G. Topole and N. Stubbs 1995 *Modal Analysis: International Journal of Analytical and Experimental Modal Analysis* **10**, 95–103. Nondestructive damage evaluation in complex structures from a minimum of modal parameters.
8. N. Stubb and J. T. Kim 1996 *American Institute of Aeronautics and Astronautics Journal* **34**, 1644–1649. Damage localization in structures without baseline modal parameters.
9. C. P. Ratcliffe 1997 *Journal of Sound and Vibration* **204**, 505–517. Damage detection using a modified Laplacian operator on mode shape data.
10. A. K. Pandy and M. Biswas 1994 *Journal of Sound and Vibration* **169**, 3–17. Damage detection in structures using changes in flexibility.
11. J. He and D. J. Ewins 1986 *Modal Analysis: International Journal of Analytical and Experimental Modal Analysis* **1**, 9–14. Analytical stiffness matrix correction using measured vibration modes.
12. O. S. Salawu and C. Williams 1995 *Journal of Structural Engineering* **121**, 161–173. Bridge assessment using forced vibration testing.
13. L. D. Peterson, S. W. Doebling and K. F. Alvin 1998 *American Society of Mechanical Engineers Journal of Vibration and Acoustics* **120**, 949–957. Experimental determination of local structural stiffness by disassembly of measured flexibility matrices.
14. M. Kaouk and D. C. Zimmerman 1994 *American Institute of Aeronautics and Astronautics Journal* **32**, 836–842. Structural damage assessment using a generalized minimum rank perturbation theory.
15. S. C. Doebling 1996 *American Institute of Aeronautics and Astronautics Journal* **34**, 2615–2621. Minimum-rank optimal update of elemental siffness parameters for structural damage identification.
16. K. M. Grigoriadis, M. O. Abdalla and D. C. Zimmerman 1998 *American Institute of Aeronautics and Astronautics Journal* **36**, 1305–1311. Enhanced structural damage detection using alternating projection methods.
17. M. Sanayei and O. Onipede 1991 *American Institute of Aeronautics and Astronautics Journal* **29**, 1174–1179. Damage assessment of structures using static test data.

18. O. Onipede, M. Sanayei and S. R. Babu 1992 *American Institute of Aeronautics and Astronautics Journal* **30**, 2299–2309. Selection of noisy measurement locations for error reduction in static parameter identification.
19. F. M. Hemez and C. Farhat 1995 *Modal Analysis: International Journal of Analytical and Experimental Modal Analysis* **10**, 152–166. Structural damage detection via a finite element models and modal updating methodology.
20. D. C. Zimmerman and M. Kaouk 1992 *American Institute of Aeronautics and Astronautics Journal* **30**, 1848–1855. Eigenstructure assignment approach for structural damage detection.
21. R. G. Cobb and B. S. Liebst 1997 *American Institute of Aeronautics and Astronautics Journal* **35**, 369–374. Sensor placement and structural damage identification from minimal sensor information.
22. D. J. Lwo, H. T. Banks, D. J. Inman and Y. Wang 1996 *Journal of Sound and Vibration* **191**, 859–880. An experimental validated damage detection theory in smart structures.
23. L. R. Deobald and R. F. Gibson 1988 *Journal of Sound and Vibration* **124**, 269–283. Determination of elastic constants of orthotropic plates by a modal analysis/Rayleigh–Ritz techniques.
24. F. Moussu and M. Nivott 1993 *Journal of Sound and Vibration* **165**, 149–163. Determination of elastic constants of orthotropic plates by a modal analysis/method of superposition.
25. E. O. Ayorinde and L. Yu 1999 *American Society of Mechanical Engineers Journal of Vibration and Acoustics* **121**, 33–40. On the use of diagonal modes in the elastic identification of thin plates.
26. A. K. Bledzki, A. Kessler, R. Rikards and A. Chate 1999 *Composite Science and Technology* **59**, 2051–2024. Determination of elastic constants of glass/epoxy uni-directional laminates by the vibration testings of plates.
27. S. K. Thyagarajan, M. J. Schulz and P. F. Pai 1998 *Journal of Sound and Vibration* **210**, 162–170. Detecting structural damage using frequency response functions.
28. W. Gawronski and J. T. Sawicki 2000 *Journal of Sound and Vibration* **229**, 194–198. Structural damage detection using modal norms.
29. H. G. Natke and C. Cempel 2001 *Journal of Sound and Vibration* **248**, 597–620. The symptom observation matrix for monitoring and diagnostics.
30. L. M. Robert 1987 *American Society for Testing Materials*. ASTM standards: C393 Test Method for Flexural Properties of Sandwich Constructions.
31. H. Y. Kim and W. Hwang 2001 *Composite Structures* **53**, 345–354. Estimation of normal mode and other system parameters of composite laminated plates.
32. L. Ljung 1987 *System Identification: Theory for the User*. NJ: Prentice-Hall, Englewood Cliffs.
33. J. N. Juang and R. S. Pappa 1985 *Journal of Control Theory and Advanced Technology* **4**, 5–14. An eigensystem realization algorithm using data correlation (ERA/DC) for modal parameter identification.
34. L. D. Peterson and K. F. Alvin 1997 *Journal of Sound and Vibration* **201**, 137–144. Time and frequency domain procedure for identification of structural dynamic models.